Angular distribution in alpha-induced fission of ^{232}Th and ^{238}U

T. Datta, S. P. Dange, H. Naik, and S. B. Manohar
Radiochemistry Division, Bhabha Atomic Research Centre, Trombay, Bombay 400 085, India
(Received 6 July 1992; revised manuscript received 25 February 1993)

The angular distribution of fission products has been measured as a function of mass asymmetry in the fissioning systems ^{232}Th($\alpha_{39.1\ \mathrm{MeV}}$,$f$), ^{238}U($\alpha_{29.0\ \mathrm{MeV}}$,$f$), and ^{238}U($\alpha_{39.1\ \mathrm{MeV}}$,$f$) using the recoil-catcher technique and off-line gamma spectrometry. The present data have been analyzed along with similar data reported earlier by us for ^{232}Th($\alpha_{29\ \mathrm{MeV}}$,$f$) and ^{233}U($\alpha_{29\ \mathrm{MeV}}$,$f$) and the literature data on mass-averaged products in the same fissioning systems in the alpha energy region 16–40 MeV. The angular anisotropies of the average symmetric and asymmetric products in these fissioning systems have been evaluated based on the transition state model assuming two fission modes with characteristic shapes and barrier heights and considering the multichance fission effect at various alpha energies. Agreements between the calculated and experimental anisotropies indicate that the angular distributions for the symmetric and asymmetric modes are determined at and beyond the corresponding second saddle points in the deformation energy surface. The effects of the multichance fission are also seen to play a significant role depending on the properties of the nuclides concerned.

PACS number(s): 25.85.Ge

I. INTRODUCTION

The angular distribution of fission or heavy-ion reaction products are investigated with multiple objectives [1]. In low- and medium-energy fission a major objective of such investigations has been the understanding of the properties of the fissioning nucleus in terms of the transition state model (TSM) [2]. According to the TSM [2], the fission fragment angular distribution is determined at the second saddle point due to the tilting mode of rotation. The tilting mode is characterized by a distribution of the quantum states defined as the projections (K) of the total spin on the symmetry (fission) axis. At above-the-barrier excitation energy fission, the K distribution is statistical. The variance of the K distribution depends on the properties of the nucleus at the saddle point [1,2]. Several authors [3–9] have shown the validity of the TSM and the importance of the fissioning nucleus' shape characteristics, excitation energy, and the effect of the pairing gap in governing the fission product angular distribution or anisotropy.

In view of the dependence of the fission product angular distribution on the saddle-point configurations which in turn depends on the mode of mass division, i.e., symmetric or asymmetric [10], the fission product angular distribution might depend on mass asymmetry. Kudo *et al.* [11] showed lower angular anisotropy for the mass-symmetric fission products compared to the asymmetric products in the ^{232}Th($p_{15\ \mathrm{MeV}}$,f) system. This observation was attributed [11] to the effects of multichance fission and two different saddle-point configurations corresponding to the symmetric and asymmetric mass divisions with different barrier heights but the same shape. Similar observations were also reported earlier by Cohen *et al.* [12] in 22 MeV proton-induced fission of ^{232}Th, ^{235}U, ^{238}U, and ^{233}U and by Kapoor *et al.* [13] in ^{235}U($n_{4\ \mathrm{MeV}}$,f). These observations were interpreted in terms of the influence of the multichance fission [12] and the existence of the different saddle-point shapes pertaining to the various mass asymmetric configurations [13]. Flynn, Glendenin, and Huizenga [14] reported anomalously low anisotropy for a single asymmetric product ^{83}Br in ^{209}Bi(α,f). Strong correlation of angular anisotropy with the mass asymmetry of fission products was also reported from this laboratory in ^{232}Th($\alpha_{29\ \mathrm{MeV}}$,$f$) [15] and ^{233}U($\alpha_{29\ \mathrm{MeV}}$,$f$) [16].

Presently, we report the experimentally determined angular anisotropies of fission products as a function of mass asymmetry in 29 MeV alpha-induced fission of ^{238}U and 39 MeV alpha-induced fission of ^{238}U and ^{232}Th. The present data have been analyzed and discussed along with the data in the literature on the mass-averaged [5–7] and mass-resolved [15,16] angular anisotropy data in the alpha-induced fission of ^{232}Th, ^{238}U, and ^{233}U over a wide range of alpha-particle energies ($\sim$16–40 MeV).

II. EXPERIMENTAL

The experiments were carried out at the 88-Inch Variable Energy Cyclotron, Calcutta using the external alpha particle beam of energy 30±0.4 and 40±0.4 MeV. Electrodeposited targets of ^{232}Th and ^{238}U (thickness $\sim$150 μg/cm^2) on superpure 25-μm-thick aluminum backed foils were used. The irradiations were carried out with a 5-mm-diam collimated alpha beam at an integral beam current of 12–16 μA h. In each irradiation the target was kept [111] at a 45° inclination with respect to the alpha beam in a cylindrical chamber of length 135 mm and diam 155 mm. The recoiling fission products were collected on six 25-μm-thick strips of aluminum catcher foils, placed on the inner wall of the chamber. The six catcher foils correspond to the six different emission angles from 90° to 20° with respect to the beam axis, each overing an azimuthal angle of 180°.

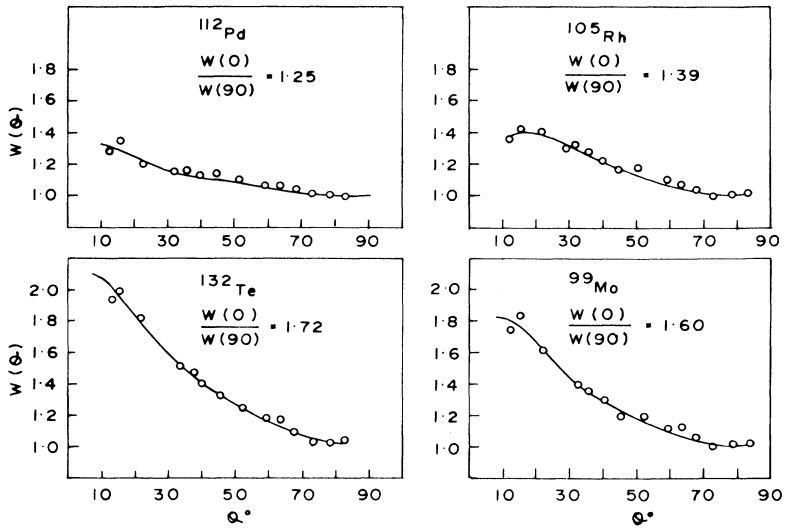

FIG. 1. Experimental angular distribution for symmetric and asymmetric products in helium ion-induced fission of ^{232}Th.

A 60 cm^3 HPGe detector coupled to a 4 K multichannel analyzer and with a resolution of 2.0 keV at 1332.0 keV was used for the off-line gamma spectrometric analysis of fission products in the various mass regions. The fission products analyzed using the well-established gamma lines were ^{91,92}Sr, ^{97}Zr, ^{99}Mo, ^{128}Sb, ^{131}I, ^{132}Te, ^{133,135}I, ^{139}Ba, and ^{141,143}Ce in the asymmetric region and ^{105}Ru, ^{112}Pd, ^{115}Cd, and ^{127}Sb in the near-symmetric region. Three irradiations were carried out for each fissioning system.

III. RESULTS

Angular anisotropy, $W(0°)/W(90°)$ for each fission product in each of the fissioning systems was deduced from the angular distribution function $W(\Theta)$ defined as

$$W(\Theta)=a+b\cos^2\Theta\ , \tag{1a}$$

$$W(\Theta)=A/\pi(\cos\Theta_i-\cos\Theta_f)\ , \tag{1b}$$

where $W(\Theta)$ is the emission probability of a specific fission product at an angle Θ per unit solid angle. $W(\Theta)$ was evaluated from the decay corrected gamma activity (A) of that product at the laboratory angle Θ within the limits Θ_i and Θ_f (the spread is due to finite catcher strip width). The laboratory angles (Θ) of measurements were 84.47°, 64.18°, 48.95°, 38.48°, 31.29°, and 25.70°. Figure 1 shows typical $W(\Theta)$ profiles for some of the asymmetric and symmetric mass fission products in ^{232}Th(α,f). For each specific fission product the angular anisotropy was deduced from least-squares fitting analysis employing Eq. (1a), in terms of the fit parameters (a and b) in each irradiation. The center-of-mass (c.m.) corrections were applied on the laboratory angles and the individual angular anisotropies in each case.

The error in the anisotropy, $W(0°)/W(90°)$, values due to the counting statistics and fitting was in the range of 5–7% while the precision was found to be within 7%. Figure 2 shows the plots of the individual fission product angular anisotropy $W(0°)/W(90°)$ averaged from three sets of measurements, as a function of mass asymmetry (A_H/A_L) in the fissioning systems ^{232}Th($\alpha_{39\ \mathrm{MeV}},f$), ^{238}U($\alpha_{29\ \mathrm{MeV}},f$), and ^{238}U($\alpha_{39\ \mathrm{MeV}},f$) and in the ^{232}Th($\alpha_{29\ \mathrm{MeV}},f$) system [15]. The mass asymmetry parameter (A_H/A_L) was deduced after correction for the prefission and postfission neutron emissions in each case as prescribed by Umezawa, Baba, and Baba [17].

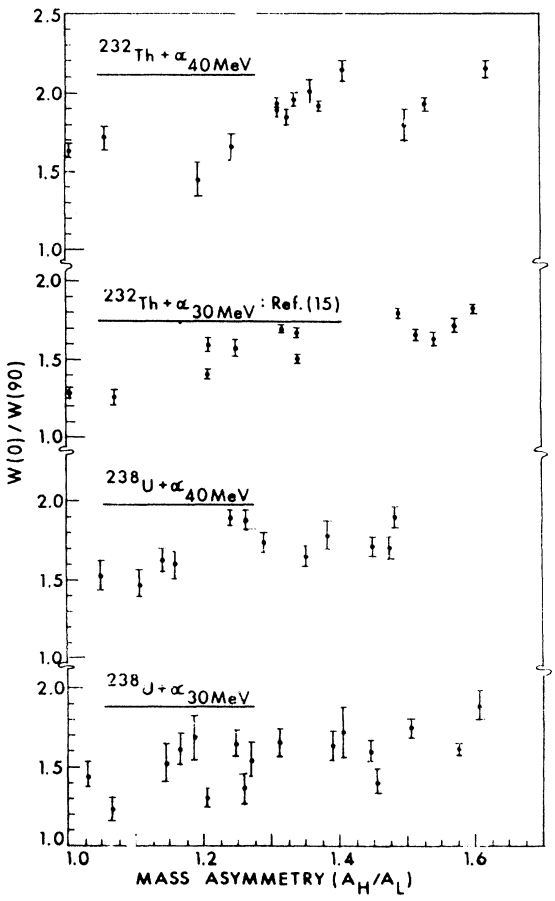

FIG. 2. Experimental angular anisotropy as a function of fission product mass asymmetry.

IV. DISCUSSION

It is seen from Fig. 2 that in both the fissioning systems ^{232}Th(α,f) and ^{238}U(α,f) the angular anisotropy of the asymmetric products are higher compared to that of the symmetric products at the alpha (bombardment) energies 29.0 and 39.1 MeV. The anisotropy is also seen to increase with the alpha energies in both the fissioning systems. The increase in the anisotropy with the energy is seen to be more in ^{232}Th(α,f) compared to that in the ^{238}U(α,f) system. The average anisotropies for the asymmetric and symmetric products in ^{232}Th(α,f) and ^{238}U(α,f) at the alpha energies 29.0 and 39.1 MeV are given in Table I in both laboratory and c.m. coordinates along with the corresponding input angular momenta ($\langle J \rangle$) and excitation energies (E^*).

It is worthwhile to recall here that several important observations on the mass-averaged fission product angular anisotropy in alpha-induced fission have been interpreted in terms of the TSM and the multichance fission (MCF) effect. These observations are stair-step behavior in anisotropy as a function of the alpha energy [5,6], sharp reduction in such stair-step behavior as well as lower gross anisotropy at higher fissility (Z^2/A) [6,18], and higher anisotropy in the alpha-induced fission compared to the neutron-induced fission at comparable excitation energies due to higher input $\langle J \rangle$ in the former case [3–5]. In view of the general understanding of the various features of the mass-averaged fission product angular anisotropy as mentioned above, an attempt was made to interpret the present observations in terms of the TSM assuming the two-mode hypothesis for the symmetric and asymmetric fission considering the effect of MCF. In this analysis we have also included our recent observations [16] in ^{233}U$(\alpha_{29\ \mathrm{MeV}},f)$.

According to the TSM in the statistical domain, $W(\Theta)$ is given by [11,19]

$$W(\Theta)=\sum_J \sigma(J)\frac{(2J+1)\exp[-(J+0.5)^2\sin^2\Theta/4K_0^2]J_0[i(J+0.5)^2\sin^2\Theta/4K_0^2]}{\mathrm{erf}[(J+0.5)/\sqrt{2}K_0]}\ , \tag{2}$$

where

$$K_0^2=I_{\mathrm{eff}}T/\hbar^2\ ,\quad I_{\mathrm{eff}}^{-1}=I_{\parallel}^{-1}-I_{\perp}^{-1}\ ,$$
$$T=[(E-Bf-E_{\mathrm{rot}})/a]^{1/2}\ , \tag{3}$$

$\sigma(J)$ is the spin (J) distribution function, J_0 is the zeroth-order Bessel function with an imaginary argument, K_0^2 is the variance of the K distribution at above-the-barrier (B_f) temperature (T) for the effective moment of inertia (I_{eff}), and $I_{\perp}$ and $I_{\parallel}$ are the moments of inertia for rotations perpendicular and parallel to the symmetry axis, respectively.

In the case of first chance fission with the spin-zero target and projectiles Eq. (3) is directly applicable with

$$\sigma(J)\approx(2J+1)T_l(E)\ ,$$

where $T_l(E)$ are the transmission coefficients for the Jth partial waves. With the onset of multichance fission, successive chance fissioning nuclei are produced with modified $\sigma(J)$ distriution at lower temperatures, i.e., K_0^2. The K_0^2 for these nuclei might be further reduced due to the superfluidity below a certain critical temperature (T_c) [9,11]. Consequently, the angular anisotropy changes in the successive chance fissions. The angular anisotropy for the symmetric and asymmetric modes might be different due to the different extents of MCF on account of the different barrier heights [10,11,20]. The mass-asymmetry dependence of the anisotropy might also arise due to the different K_0^2 values for the two modes because of different shapes since saddle-point configurations are different [10,20].

A. Calculation of multichance fission contributions

The various chance fission contributions in ^{232}Th(α,f), ^{238}U(α,f), and ^{233}U(α,f) at the different energies were

TABLE I. Anisotropy values for symmetric and asymmetric modes in ^{232}Th(α,f) and ^{238}U(α,f).

Fissioning system	^{232}Th+α		^{238}U+α	
E_α (MeV)	29.0	39.0	29.0	39.0
E^* (MeV)	23.5	33.3	23.4	33.3
$\langle J \rangle$ ($\hbar$)	9.1	13.7	9.8	13.7
Laboratory system:				
$W(0°)/W(90°)$	1.38	1.62	1.37	1.54
Symmetry	±0.13	±0.10	±0.10	±0.06
$W(0°)/W(90°)$	1.68	1.96	1.66	1.78
Asymmetry	±0.09	±0.11	±0.12	±0.09
c.m. system:				
$W(0°)/W(90°)$	1.26	1.48	1.25	1.41
Symmetry	±0.11	±0.09	±0.09	±0.06
$W(0°)/W(90°)$	1.55	1.80	1.52	1.63
Asymmetry	±0.09	±0.10	±0.11	±0.08

calculated on the basis of the ratio of fission-to-neutron emission widths (Γ_f/Γ_n) according to the standard statistical model [19,20]. The relevant input parameters for fission barrier (B_f), neutron separation energies, and level density parameters (a_n) for the different nuclides are given in Tables II–IV [21]. The Γ_f/Γ_n ratios were calculated for both the constant temperature and excitation energy-dependent level density approximations and were seen to yield similar results for the ratio of level density parameters (a_f/a_n)$\approx$1.0, in agreement with the experimental average Γ_f/Γ_n data [22].

Tables II–IV show the various chance fission contributions in the three fissioning systems at the present energies of measurements (29.0 and 39.1 MeV). In ^{232}Th(α,f) and ^{238}U(α,f) the first and the third chance fissions are predominant with comparable probabilities at both the energies. Calculations at the lower alpha energies of interest [5] showed the onset of the second chance fission at $\approx$18.5 MeV and the third chance fission at 25 MeV in these fissioning systems. In ^{233}U(α,f) the first chance fission was seen to be the most predominant (87–84 %), in excellent agreement with the experimental observations [22]. In this case the a_f/a_n ratio was used as 1.1 due to higher fissility of ^{237}Pu [6]. Calculations based on the spin-dependent Γ_f/Γ_n ratios [23] showed similar results due to the moderate $\langle J \rangle$ values in the present cases.

The calculated chance fission contributions actually refer to the asymmetric mode only since the fission barrier data used essentially correspond to the predominant asymmetric fission of the actinides [21]. The calculated fission barriers for the symmetric mode are usually 1.5–2.0 MeV higher than the corresponding asymmetric mode barriers [20]. MCF calculations showed the symmetric component to be primarily due to the first chance fission as expected [11].

B. Evaluation of K_0^2 for the symmetric and asymmetric modes

Appropriate K_0^2 values for the symmetric and asymmetric modes in each chance-fission nuclide are required to deduce the angular anisotropies for the individual modes in the fissioning systems ^{232}Th(α,f), ^{238}U(α,f), and ^{233}U(α,f). For this purpose the rigid body moments of inertia $I_\perp$ and $I_\parallel$ for the individual modes in each case were calculated using the "Funny Hills" shape parameters $\{c,h;\alpha\}$ [24]. In this approach the deformation energy of the nucleus consists of the liquid-drop energy with the shell and pairing corrections and the shape is described in terms of the following parameters: elongation (c), neck constriction (h), and mass asymmetry (α). The parameter α is related to the mass asymmetry (A_H/A_L) as [25]

$$\frac{A_H}{A_L}=\frac{1+3\alpha c^3/8}{1-3\alpha c^3/8} . \tag{4}$$

In the actinide region these shape parameters are nearly constant and the fission barriers are essentially due to the single-particle effects [24,25]. Accordingly, the elongation c is $\approx$1.6 at the saddle point and $\approx$1.75 near the scission for the actinides remaining unaffected by the h and α values. For the symmetric shape (α=0.0) saddle point, h is -0.05 to -0.075 at $c\approx1.60$ [24]. The energy of the outer barrier is lowered due to the shell effects for the asymmetric shapes ($\alpha>0.0$) and the asymmetric saddle point of the lower barrier is obtained for slightly

TABLE II. Multichance fission, K_0^2, and various input parameters in ^{232}Th(α,f).

Fissioning nuclide	^{236}U	^{235}U	^{34}U	^{233}U
a_n/MeV	28.51	29.05	26.79	29.05
B_f (MeV)	5.54	5.90	5.50	5.80
S_n (MeV)	6.54	5.31	6.84	5.79
E_c (MeV)	18.8	6.8	20.5	6.5
Asymm.: $I_{\perp R}$ ($\hbar^2$/MeV)	321.10	318.20	315.20	312.20
Mode: $I_{\parallel R}$ ($\hbar^2$/MeV)	69.45	69.18	68.91	68.66
Symm. $I_{\perp R}$ ($\hbar^2$/MeV)	218.80	217.30	215.80	214.80
Mode: $I_{\parallel R}$ ($\hbar^2$/MeV)	76.85	76.31	75.77	75.23
	At E_α=29.0 MeV, $J_{max}=12.9\hbar$			
E^* (MeV)	23.5	15.0	8.3	
$\langle J \rangle$ ($\hbar$)	9.1	8.6	7.9	
% Fission	42.8	7.1	50.1	
K_0^2: Asym.	69.6	48.6	13.2	
Symm.	93.1	64.7	16.2	
	At E_α=39.1 MeV, $J_{max}=19.4\hbar$			
E^* (MeV)	33.3	24.6	17.4	8.4
$\langle J \rangle$ ($\hbar$)	13.7	12.2	10.9	9.9
% Fission	38.1	8.5	44.3	9.1
K_0^2: Asym.	86.3	69.5	57.0	22.5
Symm.	115.3	92.5	75.5	29.6

TABLE III. Percentage of multichance fission, K_0^2 and various input parameters in $^{238}U(\alpha,f)$.

Fissioning nuclide	^{242}Pu	^{241}Pu	^{240}Pu	^{239}Pu
a_n/MeV	29.00	28.50	27.41	28.00
B_f (MeV)	5.10	5.50	5.07	5.70
S_n (MeV)	6.30	5.24	6.52	5.66
E_c (MeV)	16.9	5.1	14.1	5.1
Asymm.: $I_{\perp R}$ ($\hbar^2$/Mev)	335.40	332.40	329.40	326.40
Mode: $I_{\parallel R}$ ($\hbar^2$/MeV)	72.23	71.95	71.68	71.42
Symm.: $I_{\perp R}$ ($\hbar^2$/MeV)	228.20	226.60	225.10	223.50
Mode: $I_{\parallel R}$ ($\hbar^2$/MeV)	80.14	79.59	79.04	78.49
At $E_\alpha=29.0$ MeV, $J_{max}=13.8\hbar$				
E^* (MeV)	23.4	15.3	8.6	
$\langle J\rangle\hbar$	9.0	8.5	7.9	
% Fission	47.3	9.2	43.5	
K_0^2: Asym.	72.4	52.9	25.9	
Symm.	97.2	70.6	33.7	
At $E_\alpha=39.1$ MeV, $J_{max}=19.4\hbar$				
E^* (MeV)	33.3	24.9	17.8	9.7
$\langle J\rangle\hbar$	13.7	12.5	11.7	11.0
% Fission	41.7	10.4	41.1	6.8
K_0^2: Asym.	89.6	74.2	60.4	30.6
Symm.	120.2	99.1	80.3	40.5

lower elongation at $h\approx0.0$. The α value for the asymmetric mode varies between 0.11 and 0.14 on the basis of the mass distribution systematics in actinide fission (average heavy mass peak at $A\approx140$). It is also established that for the asymmetric shapes at $h<0.75$ pronounced neutron shell effects lead to a lower-energy path from around the second minimum to the exit valley at $c\approx1.70$ prior to the scission.

In view of these considerations the $\{c,h\}$ parameters used to define the shapes of all the concerned nuclei were $\{1.60,-0.075\}$ for the symmetric mode ($\alpha=0.0$) and $\{1.75,0.027\}$ for the asymmetric mode with α value varying from 0.11 to 0.14. The rigid body moments of inertia $I_{\perp R}$,$I_{\parallel R}$ for the individual modes were then calculated in each case as [25]

TABLE. IV. Percentage of multichance fission and various input parameters energy in $^{233}U(\alpha,f)$.

Fissioning nuclide	^{237}Pu	^{236}Pu
a_n/MeV	29.05	28.51
B_f (MeV)	5.20	4.50
S_n (MeV)	5.90	7.36
E_c (MeV)	5.20	19.1
Asymm.: $I_{\perp R}$($\hbar^2$/MeV)	324.10	321.10
Mode: $I_{\parallel R}$($\hbar^2$/MeV)	69.72	69.45
Symm.: $I_{\perp R}$ ($\hbar^2$/MeV)	220.40	218.80
Mode: $I_{\parallel R}$ ($\hbar^2$/MeV)	77.40	76.85
At 20.0 MeV, $J_{max}=12.5\hbar$		
E^* (MeV)	22.8	15.1
$\langle J\rangle$ ($\hbar$)	8.8	8.2
% Fission	84.0	16.0
K_0^2: Asym.	68.5	53.2
Symm.	92.0	71.2

$$I_{\parallel R}=\frac{1}{c}+\frac{c^2f(c^3f/3-1)}{7}+\frac{c^5\alpha^2}{7},$$
$$I_{\perp R}=\frac{c^2}{2}+\frac{1}{2c}+\frac{c^2f(c^3+c^3f/6-0.5)}{7}-0.5c^5\alpha^2(c^3/5-1/7) \quad (5)$$

for

$$f=0.8\{2h+(c-1)/2\}$$

in terms of I_0, the spherical moment of inertia.

The K_0^2 values calculated using Eqs. (3) and (7) need corrections for the superfluidity due to the BCS pairing interaction depending on the temperature (T). In case T is below the critical temperature (T_c) of a nucleus, the pairing interaction modifies the spectrum of the independent particle states [9] reducing the K_0^2 due to the contribution of the states only above a minimum energy, i.e., the pairing gap (δ). In the superfluid condition ($T<T_c$) the K_0^2 is [9]

$$K_0^2=\frac{I_{\perp R}I_{\parallel R}f(T/T_c)A(T/T_c)}{I_{\perp R}f(T/T_c)-I_{\parallel R}A(T/T_c)}\frac{T}{\hbar^2}, \quad (6)$$

where $T_c=\frac{4}{7}\delta$ and the critical energy $E_c=1.473aT_c^2$.

For all the nuclei, the gap parameters (δ) were taken from the literature [21,26]. The temperature-dependent integrals $A(T/T_c)$ and $f(T/T_c)$ were also taken from the standard tables [9,19]. The K_0^2 values for the symmetric and asymmetric modes in each nuclei were evaluated at the different energies using the superconductor model. The T_c, E_c, and K_0^2 values (for the present alpha energies) are given for the different chance-fission nuclei in the Tables II–IV.

C. Evaluation of angular anisotropy and results

In each fissioning system at each energy the net anisotropy for the asymmetric mode was evaluated as the chance-fission-contribution weighted average of the asymmetric mode anisotropies for the individual chance-fission nuclei. For the symmetric mode only the first chance fissioning nucleus was considered. To calculate the anisotropy in each case the appropriate K_0^2 values were used in Eq. (2) with a modified spin distribution $\sigma(J)$ following neutron emission (for higher chance nuclei) but assuming the total spin (J) perpendicular to the beam direction ($M=0$). The latter assumption is valid, on the average, as long as neutron emission is very nearly isotropic and for large initial and total spin (J) [13]. The modified (broader) distribution was calculated according to the statistical model using the Haffner-Huizenga-Vandenbosch code [27] as

$$\sigma(J)\approx \sum_{J=0}^{J_{\max}} P(J_i)(2J+1)\exp\left[-\frac{(J+0.5)^2}{2\sigma_n^2}\right] \times \sum_{S=|J-s|}^{J+s} \sum_{l=|J-S|}^{J+S} T_l(E_n)\,, \tag{7}$$

for

$$P(J_i)\approx \sum_{S=|I-s|}^{I+s} \frac{2Ji+1}{(2I+1)(2s+1)} \sum_{l=|Ji-S|}^{J_i+S} T_l(E_\alpha) \tag{8}$$

$P(J_i)$ is the initial spin distribution with I and s as the target and projectile spins, respectively. $T_l(E_n)$ and $T_l(E_\alpha)$ are the optical-model transmission coefficients for the neutron and alpha particles, respectively, evaluated based on the potentials as prescribed in Refs. [5,6]. σ_n is the spin cutoff factor. The experimental data for the mass-averaged and mass-resolved fission product angular anisotropies from the literature [5–7] and from this laboratory in the fissioning systems ^{232}Th(α,f), ^{238}U(α,f), and ^{233}U(α,f) in the alpha energy range 16–40 MeV are compared against the calculated anisotropies in Fig. 3.

It is seen from Fig. 3 that the following can be concluded. (a) Angular anisotropies at the different energies as well as fluctuations due to the MCF are well reproduced by the theoretical calculations in all the cases. (b) The agreement between the calculated and experimental anisotropies for the symmetric and asymmetric modes in all three systems clearly show that the two modes have intrinsically different angular distributions governed by the corresponding configurations with characteristic shapes and barrier heights. Such shape dependence is further apparent from the mass-asymmetry dependence of the anisotropy in ^{233}U(α,f) where the MCF effect is not significant. (c) For the symmetric mode in all the systems, close agreement between the calculated and experimental anisotropies confirms the absence of the higher chance fission. (d) The stair-step behavior in the calculated anisotropy with the input energy is seen to decrease with increasing fissility as observed. (e) sharper fluctuations due to the MCF effect occurs in the nuclei with high E_c (^{236}U > ^{242}Pu) due to the superfluidity. In the light of the above analysis and the observations (a)–(e) it is apparent that the present attempt is reasonably successful in interpretation of the mass-averaged and mass-resolved angular distributions of the fission products in the medium-energy fission of the actinides considered. The present approach shows the importance of both the symmetric saddle point and the near-scission asymmetric shapes compared to the recent models [28] to interpret the fission produce angular distributions in terms of either the saddle point or the scission configurations.

The following conclusion can be drawn. (a) Experimental investigations on the individual fission product angular distributions in the fissioning systems ^{232}Th(α,f), ^{238}U(α,f), and ^{233}U(α,f) at $E_\alpha=29$ and 39 MeV have clearly shown a mass-asymmetry dependence of the angular distribution with higher anisotropy for the asymmetric fission products compared to the symmetric ones. (b) Theoretical analysis employing the transition-state model assuming the two-mode hypothesis and considering the multichance fission effect shows that angular anisotropies of the symmetric and asymmetric modes are

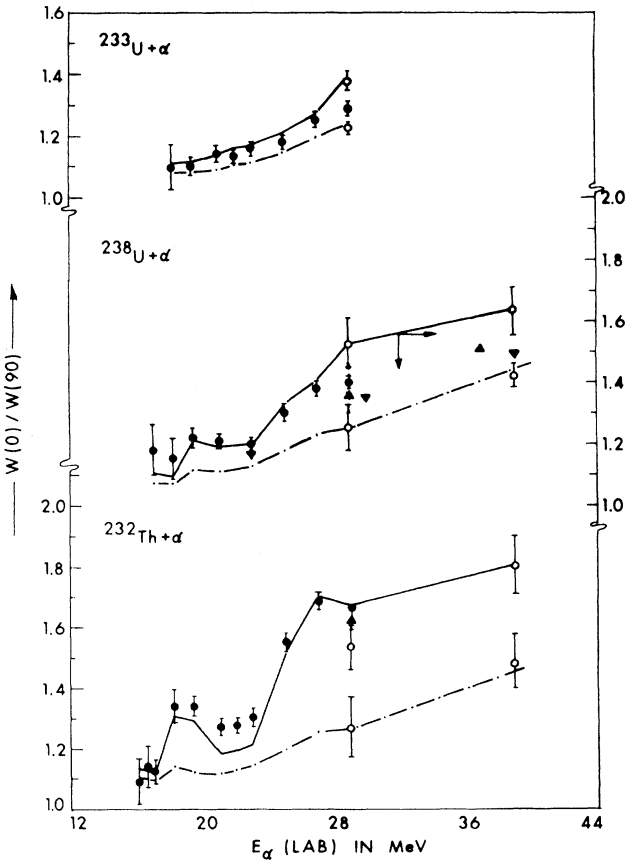

FIG. 3. Comparison of theoretical and experimental angular anisotropy in ^{232}Th(α,f), ^{238}U(α,f), and ^{233}U(α,f) Experimental Data: This laboratory, Ref. [6], Ref. [6], and Ref. [17]. Theoretical plots: ----asymmetric mode; symmetric mode.

governed by the characteristic configurations at the symmetric saddle point and well past the asymmetric saddle point, respectively. (c) The present approach is able to interpret the experimentally observed mass-resolved and mass-averaged angular anisotropies in the medium-energy ($E_\alpha = 16-40$ MeV) fission of the actinides.

ACKNOWLEDGMENTS

The authors acknowledge the keen interest shown by Dr. R. H. Iyer, Radiochemistry Division, BARC, in this work. They are thankful to the VECC crew and Dr. S. K. Saha for their excellent support in the experiments.

[1] L. C. Vaz and J. M. Alexander, Phys. Rep. **97**, 1 (1983).
[2] A. Bohr, in *Proceedings of the International Conference on Peaceful Uses of Atomic Energy* (United Nations Publications, Geneva, 1957), Vol. 2, p. 131; I. Halpern and V. M. Strutinski, *ibid.*, p. 398.
[3] J. E. Simmons and R. L. Henkel, Phys. Rev. **120**, 198 (1906).
[4] J. E. Simmons, R. B. Perkins, and R. L. Henkel, Phys. Rev. **137**, B809 (1961).
[5] R. B. Leachman and L. Blumberg, Phys. Rev. **137**, B814 (1965).
[6] R. Vandenbosch, H. Warhaneck, and J. R. Huizenga, Phys. Rev. **124**, 846 (1961).
[7] S. S. Kapoor, H. Baba, and S. G. Thompson, Phys. Rev. **149**, 965 (1966).
[8] L. Blumberg and R. B. Leachman, Ann. Phys. **18**, 274 (1962).
[9] J. J. Griffin, Phys. Rev. **132**, 2204 (1963).
[10] P. Moller and S. G. Nilsson, Phys. Lett. **31B**, 283 (1970).
[11] H. Kudo, Y. Nagame, H. Nakahara, K. Miyano, and I. Kohno, Phys. Rev. C **25**, 909 (1982).
[12] B. L. Cohen, B. L. Ferrel-Bryan, D. T. Coombe, and M. K. Hullings, Phys. Rev. **98**, 68 (1955).
[13] S. S. Kapoor, D. M. Nadkarni, R. Ramanna, and P. N. Ramarao, Phys. Rev. **137**, B511 (1965).
[14] K. F. Flynn, L. E. Glendenin, and J. R. Huizenga, Nucl. Phys. **58**, 321 (1964).
[15] S. B. Manohar, T. Datta, A. Goswami, and Satya Prakash, in *IAEA Symposium on Physics and Chemistry of Fission,* Gaussing, Dresden, edited by H. Martin and D. Seeliger (ZFK Publication, Dresden, 1988).
[16] A. Goswami, S. B. Manohar, S. K. Das, A. V. R. Reddy, B. S. Tomar, and Satya Prakash, Z. Phys. A **342**, 299 (1992).
[17] S. Umezawa, S. Baba, and H. Baba, Nucl. Phys. **A160**, 65 (1971).
[18] C. T. Coffin and I. Halpern, Phys. Rev. **112**, 536 (1958).
[19] R. Vandenbosch and J. R. Huizenga, Nuclear Fission (Academic, New York, 1974).
[20] C. F. Tsang and J. B. Wilhelmy, Nucl. Phys. **A184**, 417 (1972).
[21] S. Bjornholm and J. E. Lynn, Rev. Mod. Phys. **52**, 725 (1980).
[22] T. D. Thomas, B. G. Harvey, and G. T. Seaborg, in *Proceedings of the International Conference on Peaceful Uses of Atomic Energy* (United Nations Publications, Geneva, 1985), Vol. 15, p. 295.
[23] T. Dossing and J. Randrup, Nucl. Phys. **A433**, 215 (1985).
[24] R. W. Hasse and W. D. Myers, *Geometrical Relationships of Macroscopic Nuclear Physics* (Springer-Verlag, Berlin, 1988), p. 78–82.
[25] M. Brack, J. Damgaard, A. S. Jensen, H. C. Pauli, V. M. Strutinskii, and C. Y. Wong, Rev. Mod. Phys. **44**, 320 (1972); H. C. Pauli, Phys. Rep. **7**, 35 (1973).
[26] A. Gilbert and A. G. W. Cameron, Can. J. Phys. **43**, 1446 (1965).
[27] W. L. Haffner, Jr., J. R. Huizenga, and R. Vandenbosch, ANL Report No. 6662, 1962 (unpublished); T. Datta, S. P. Dange, H. Naik, and Satya Prakash, Phys. Rev. C **46**, 1445 (1992).
[28] P. D. Bond, Phys. Rev. C **32**, 471 (1985); B. B. Back, S. Bjornholm, T. Dossing, W. Q. Shen, K. D. Hildenbrand, A. Gobbi, and S. P. Sorensen, *ibid.* **41**, 1495 (1990).